e-Polymers **2009**, no. 029

http://www.e-polymers.org

ISSN 1618-7229

Self-assembly in the solutions of poly(methyl methacrylates) end-capped with fluorophenyl groups

Ekaterina R. Gasilova,[1] Olga G. Zakharova,[2] Sergey D. Zaitsev, Yury D. Semchikov[2]*

[1*]Institute of Macromolecular Compounds, Russian Academy of Sciences, Bolshoy pr., 31, 199004, St.-Petersburg, Russia; fax 7 812 328 68 69, e-mail: gasilova@hotmail.com

[2] N. I. Lobachevsky Nizhny Novgorod State University, pr. Gagarina, 23, building 2, 603950, Nizhny Novgorod, Russia; fax 7 831 465 85 92; e-mail: emchikov@ichem.unn.ru

(Received: 11 September, 2008; published: 20 March, 2009)

Abstract: Self-assembly of poly(methyl methacrylates) end-capped with -Ge(C_6F_5)$_3$ groups (PMMA-F) has been studied in a selective solvent (acetone) by means of photon correlation spectroscopy and static light scattering. PMMA-F's of different molecular weights (MW), were obtained by radical polymerization in the presence of a chain transfer agent, HGe(C_6F_5)$_3$. At MW>130 000 conformational and hydrodynamic properties of PMMA-F's is shown to be the same as of PMMA. At MW less than130 000 an aggregation starts: additional fraction of large scatterers appears in PCS. Large aggregates of R_h=200 - 300 nm are likely to be formed by bridged micellar clusters. Presence of large aggregates indicates a super strong segregation limit predicted in the work of Semenov et al.

Keywords: self-assembly, partially fluorinated polymers, end-capped polymers, light scattering; photon correlation spectroscopy

Introduction

Since incorporation of fluorinated fragments alters dielectric, optical and frictional properties of macromolecules, there is an increasing interest in such polymers. Self-assembly of partially fluorinated oligomers and polymers is a promising way of designing materials [1, 2]. Among partially fluorinated polymers, block copolymers containing fluorinated block have been mostly studied [3-8]. It is well recognized that their self-assembly is governed by the incompatibility of fluoro- and hydrocarbons. Fluorination of one of the blocks has been shown by Lodge et al. to increase strongly the Flory-Huggins interaction parameter χ of blocks and, therefore, to influence the phase behavior [5-9]. The [7] phase diagrams of partially fluorinated block-copolymers were not described by the self-consistent mean-filed theory, which is working in hydrocarbon block-copolymers. Instead, partially fluorinated block-copolymers were shown to exhibit a super strong segregation limit (SSSL) proposed in the work of Semenov et al [10]. According to [10], SSSL exists at high values of segregation parameter χN>>100, where N is the overall polymerization degree. It was shown [10] that in selective solvent SSSL can result in non-spherical large micelles even at low fraction of insoluble component.

Present work concerns hydrocarbon flexible polymers end-capped with fluorinated groups. Interest to end-functionalized polymers increased in the last years due to their practical significance [11]. Oligomers end-capped with fluoroalkyl groups were

shown to behave as surfactants in organic solvents, and in the super-critical CO_2 [12-14].

We present the study of self-assembly of PMMA-Fs - poly(methyl methacrylates) end-capped with [$Ge(C_6F_5)_3$] groups - in acetone solutions. We have explored the influence of MW (and, hence, of the content of insoluble end-groups) on the aggregation ability of PMMA-Fs. By means of static light scattering (SLS) and PCS, conformational, thermodynamic, and hydrodynamic properties of PMMA-Fs were investigated in solution.

This work continues the studies of aggregation in the solutions of block-copolymers PMMA-co-PPG, where PPG is a hyper branched perfluorinated poly(phenylene german) [8, 9, 15-18]. Aggregation of these block-copolymers in solutions was shown to take place by means of SLS and PCS [8, 9]. In the solid state, their aggregation has been confirmed by means of atomic force microscopy [18]. In [8] we have shown that aggregation of PMMA-co-PPG strongly depends on the solvent. Terminal and middle fluorinated groups of PPG are [$(C_6F_5)_3$] and [C_6F_4], respectively. Therefore, PPG was used as a fluorinated polymer, modeling the behavior of [$Ge(C_6F_5)_3$] end-groups of PMMA-F. To choose an efficient selective solvent, we looked for the worst solvent for PPG among good solvents for PMMA. The preliminary choice has been done on the base of PCS studies in acetone, chloroform, and THF solutions of PPG [17].

Results and discussion

R_h-distributions

Molecular masses of the polymers characterized by SEC are listed in Tab. 1, Section 4.2. While analyzing the PCS results, we noticed that upon lowering the molar mass of PMMA-F, distributions of their R_h qualitatively change from unimodal to bimodal ones. At MW>130 000 the R_h-distributions are unimodal. An example of unimodal distribution is presented for the PMMA-F_{III} solution in Fig. 1. Further on in the Section, we shall show that the pick position corresponds to R_h of individual macromolecules.

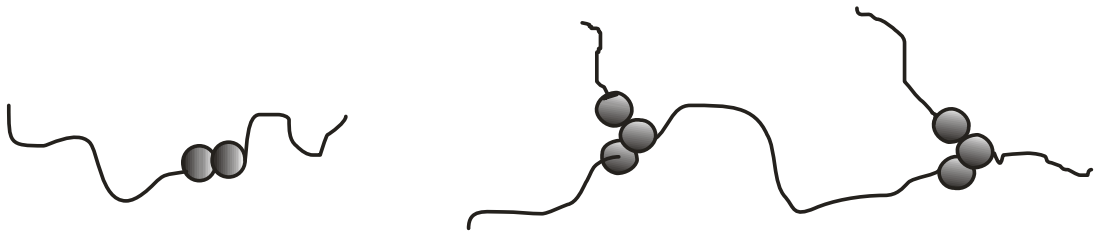

1 2

Scheme 1. Possible aggregates in PMMA-F's of MW≤M_{crit}. Small scatterers as the low-order multimers are shown in (1); a fragment of large scatterers is shown in (2). We have specified that LAs can contain PMMA-Fs end-capped by both ends.

As the molar mass of PMMA-F decreases, additional maximum, manifesting large aggregates (LA), appears. First indications of aggregation are observed in PMMA-F_V solutions, i.e. at MW=131 000. The fraction of the LA-mode, i.e. the relative area

under its maximum, is low. As MW decreases, the fraction of LA increases (Fig. 1). Large aggregates were observed in the PMMA-F solutions at MW≤M_{crit}≈130 000. Further on all parameter determined for the small scatterers will be named by subscribe “s”, for the large scatterers - by subscribe “L”. Fig. 1 shows an increase of the LA-fraction upon decreasing MW of PMMA-F. By extrapolation to infinite dilution, we obtained R_{hL}=250, 220 and 290 nm for PMMA-F_V, PMMA-F_{VI}, and PMMA-F_{VII}, respectively.

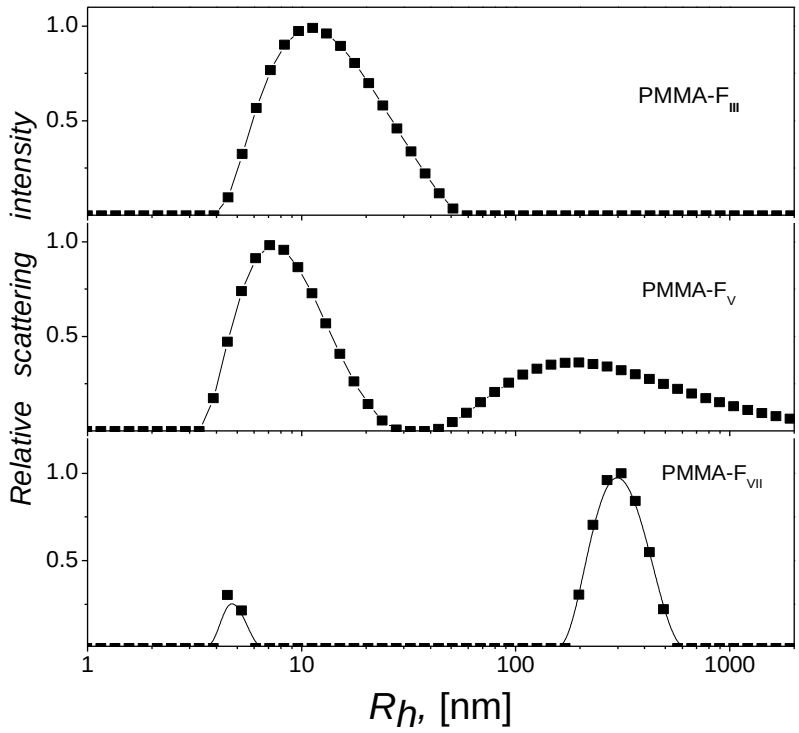

Fig. 1. Examples of R_h-distributions of PMMA-F. PCS was performed at the scattering angle θ=40°. Concentrations of PMMA-F_{III}, PMMA-F_V, and PMMA-F_{VII} in acetone were 2.38, 6.36, and 8.54 g/l, respectively.

Further down we shall demonstrate that the small scatterers of aggregated solutions are rather not individual macromolecules of PMMA-F, but their low-order multimers. Possible structures of the small and large scatterers are shown in Scheme 1. In this scheme PMMA-Fs end-capped with [$Ge(C_6F_5)_3$] groups at one end, and at both ends are presented. These two types of end-capped PMMA-Fs are due to two mechanisms of chain termination in radical polymerization (disproportionation and recombination, respectively). According to [16], the content of PMMAs end-capped by one and both ends is 70% and 30%, respectively. In the Scheme 1 we have illustrated that PMMA-F end-capped at both ends can form bridges between micelles in LAs.

SLS

A specific refractive index increment (ν) of PMMA-F solutions showed a molar mass dependence. A linear fit of $\nu=f(1/M)$ in the studied range of MWs resulted in

ν=0.1226+1439/M_w*(SEC),* [cm^3/g]. In PMMA ν=0.1277 cm^3/g did not depend on MW. Independence of ν on MW is normal for hydrocarbon polymers; only in hydrocarbon oligomers the same kind of molar mass dependence ($\nu \propto 1/M$) was observed [19]. The molecular mass dependence of ν is an indication of the appreciable role of $Ge(C_6F_5)_3$ end-groups in acetone solutions of PMMA-F.

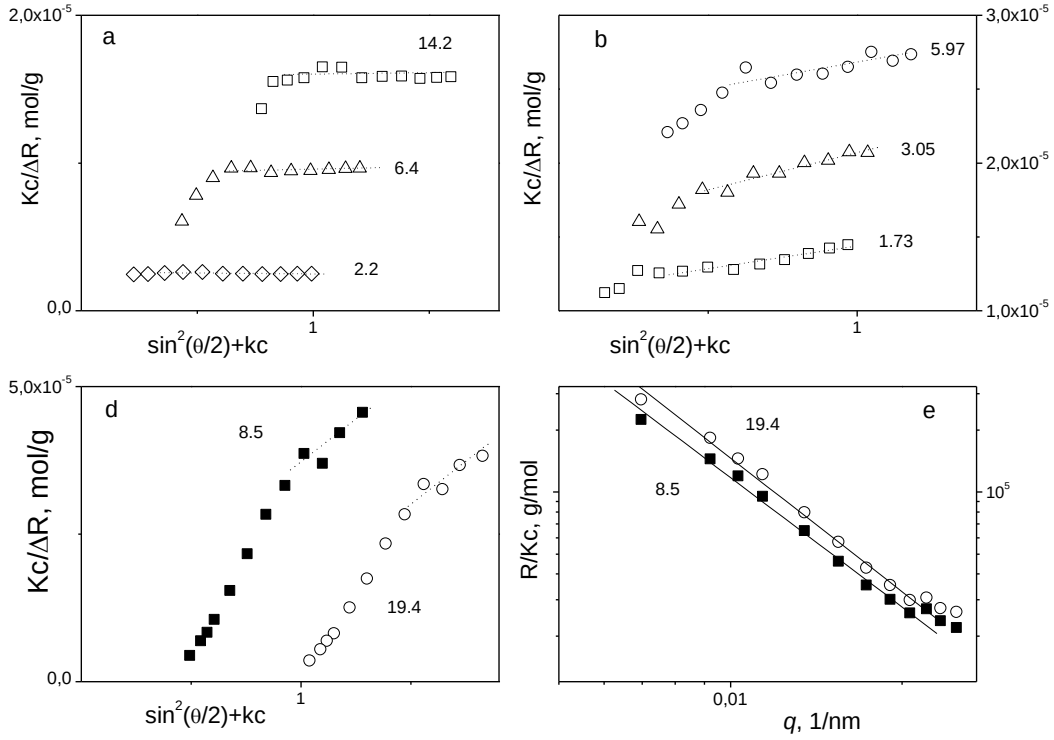

Fig. 2. Concentration and angle dependences of *Kc/ΔR* of aggregated PMMA-F_V (Fig. 2a), PMMA-F_{VI} (Fig. 2b), and PMMA-F_{VII} (Figs 2d) in acetone plotted in the Zimm coordinates (eq. 1). Everywhere k=0.05. Dotted lines represent the linear high-angle parts of the Zimm diagrams used in determination of A_{2s}, M_s, and R_{gs}. In Fig. 2e, lg ($\Delta R/Kc$) of PMMA-F_{VII} is plotted *vs.* lg q. The solid lines represent the least-square fits of the low-angle parts. Concentrations in g/l indicate the curves.

We found that Zimm diagrams of PMMAs and of non-aggregated PMMA-Fs were linear. In aggregated solutions of PMMA-F_V, PMMA-F_{VI}, an enhanced excess low-angle scattering was observed: the Zimm diagrams were bent down at low scattering angles. This behavior is demonstrated for the PMMA-F_V and PMMA-F_{VI} solutions (Figs. 2a and 2b, respectively). Distortions of the Zimm diagrams shown in Figs. 2a, 2b manifest the presence of small fraction of large scatterers [19, 20]. In the Zimm diagram of the lowest studied homologue, PMMA-F_{VII}, scattering from LAs becomes predominant over almost all range of θ (Fig. 2d). In the next section the R_{gs} of PMMA-F_V, PMMA-F_{VI} will be presented. We were not able to determine the R_{gL} values, since for LAs qR_{gL}>1. In PMMA-F_{VII} it is possible to get information on the inner structure of LAs by plotting lg($\Delta R/cK$) vs. lg q (Fig. 2e). Least-square fits of these dependences give $\Delta R \propto q^{-d}$, *where* $d \approx 2.1$ is related to the fractal dimension of LAs.

Thus, the PCS and SLS indications of aggregation are in accord with each other: enhanced low-angle scattering in SLS is accompanied by the appearance of additional R_h-maximum of large scatterers in PCS. In aggregated PMMA-Fs, both methods manifest the increasing role of LAs with decreasing MW of PMMA-F.

Lower aggregation thresholds M_{crit} were observed in the other end-capped polymers [12, 21]. In particular, polystyrenes end-capped with perfluoroalkyl groups [$(CF_2)_{13}F$] demonstrated aggregation in benzene at M_{crit}=5000 [12]. Thus, [$Ge(C_6F_5)_3$] groups are more effective in aggregation than perfluoroalkyl ones.

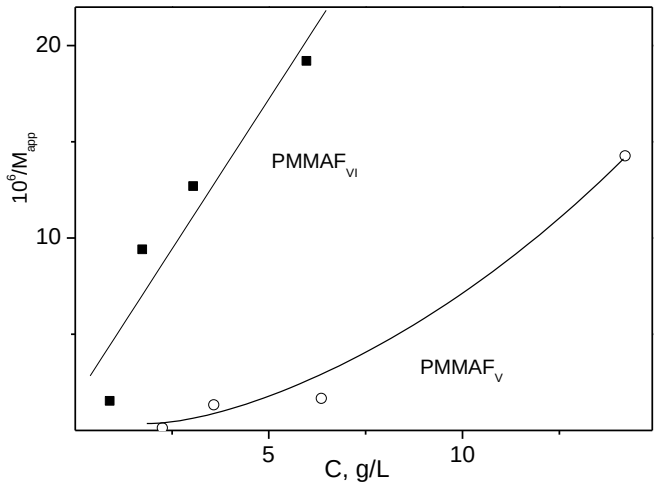

Fig. 3. Concentration dependences of $1/M_{app}$ in the PMMA-F_V and PMMA-F_{VI} acetone solutions.

In the aggregating solutes, concentration dependence of an apparent molecular mass M_{app} is often analyzed, where $1/M_{app}=(Kc/\Delta R)_{\theta\to 0}$. Minimum of $1/M_{app}=f(c)$ at a critical aggregation concentration (CAC) is observed [20, 22-23]. An increase of $1/M_{app}$ with concentration at c>CAC is due to the micelle-micelle repulsive interactions. At c<CAC the increasing fraction of micelles dominates the M_{app} behavior. Thus the slope of $1/M_{app}=f(c)$ gives an apparent A_2, reflecting not only the virial term but the aggregation process as well.

Concentration dependences of $1/M_{app}$ are plotted in Fig. 3. for the PMMA-F_V and PMMA-F_{VI} solutions. As we have already noticed, the low-angle parts of the Zimm diagrams of Fig.2 are governed by the large scatterers. Thus Fig. 3 concerns mainly the LAs. Fig. 3 shows that in PMMA-F_V solutions $1/M_{app}=f(c)$ flattens at lower ***c***, but the minimum (i.e. the CAC) is not reached. In PMMA-F_{VI} solutions we see only how $1/M_{app}$ increases with concentration. Probably, these differences mean that CAC(PMMA-F_{VI})<CAC(PMMA-F_V). In PMMA-F_{VI} solutions, the slope of the $1/M_{app}=f(c)$ dependence is higher than in PMMA-F_V solutions. Thus A_{2L}(PMMA-F_{VI})>A_{2L}(PMMA-F_V).

Low CACs in the studied set of PMMA-Fs are a consequence of high MW of aggregating PMMA-Fs. It is known, that critical micelle concentrations of traditional surfactants (which MW is low) are higher than CACs of block-copolymers [24], because the increase of the surfactants MW stabilizes micelles.

Further on in aggregated PMMA-Fs we shall pay attention to the high-angle linear part of Zimm diagrams. However, these results depend on the choice of suitable angles where the small scatterers are dominant. Lines in Fig. 2. indicate this range. For broad unimodal distribution this procedure would lead to $M=2M_n$ [20]. In our case, the distribution of scatterers in aggregated PMMA-F was distinctly bimodal. Therefore, we assumed that high-angle parts of Zimm diagrams describe mainly the small scatterers, their molar masses, gyration radiuses, and apparent virial coefficients (M_s, R_{gs}, A_{2s}, respectively).

Tab. 1. Comparison of MWs determined by SLS and SEC.

Sample	k^a	$k_L{}^b$	$k_s{}^c$
$PMMA_I$	1.0		
$PMMA_{II}$	1.0		
$PMMA_{III}$	1.2		
$PMMA\text{-}F_I$	1.2		
$PMMA\text{-}F_{II}$	1.2		
$PMMA\text{-}F_{III}$	0.9		
$PMMA\text{-}F_{IV}$	1.3		
$PMMA\text{-}F_V$		>>1	4.2
$PMMA\text{-}F_{VI}$		>>1	2.5
$PMMA\text{-}F_{VII}$		>>1	1.2

[a] $k=M_w(SLS)/M_w(SEC)$ - for PMMAs and non-aggregated PMMA-Fs;
[b] $k_s=M_s(SLS)/M_w(SEC)$ - in aggregated PMMA-Fs. Molecular mass of small scatterers (M_s) was determined from the high-angle part of Zimm diagrams;
[c] $k_L=M_L/M_w(SEC)$ – in aggregated PMMA-Fs. Molecular mass of large scatterers (M_L) was determined from the low-angle part of Zimm diagrams.

Tab. 1 lists the comparison of MWs determined by SEC and SLS. It follows from Tab. 1, that in non-aggregated PMMA-F and in PMMA MW(SEC) and MW(SLS) are equal within 30%. In the solutions of PMMA-F (V-VII) SEC chromatograms did not show the second maximum of LA. Thus the eluent (THF at 40 ^oC) is a non-selective solvent for the whole set of PMMA-Fs. In fact, during the choice of a proper selective solvent, we have noticed that THF does not produce LAs of the corresponding perfluorinated polymer PPG, as opposite to acetone, where mainly the LAs of PPG were observed [17].

The SLS-analyses of the small scatterers give MW values close to those obtained by SEC: k_s=1÷4. Minding the uncertainty of choosing the high-angle part of Zimm diagrams responsible for the small scatterers, from this data we cannot say whether the small scatterers are individual macromolecules or their low-order multimers with the aggregation degree $\approx k_s$. Therefore, in the next section we shall examine, whether R_{gs}, $A_{2s,}$ and R_{hs} differ from the corresponding values expected for PMMA.

Molecular mass dependences of R_g, R_h and A_2

Comparison of molecular mass dependences $R_g(M_w)$, $R_h(M_w)$ of non-aggregated PMMA-F and PMMA, with those of the small scatterers of aggregated PMMA-Fs is

demonstrated in Fig. 4 (a, b). Each abscissa in Fig. 4 corresponds to different PMMA, and PMMA-F samples. For the small scatterers of PMMA-F_V, PMMA-F_{VI}, PMMA-F_{VII}, M_s= 675000, 140000 and 67000, respectively.

Let us consider first the $R_g(M_w)$ dependences in the acetone solutions of PMMA and PMMA-F, shown in Fig. 4a. Line α shows the result of calculation of R_g of PMMA:

$$\sqrt{R_g^2} = A\sqrt{n^{1+\varepsilon}/6} \qquad (1)$$

where A is the Kuhn segment length, n is the number of Kuhn segments in a macromolecule, ε accounts for the excluded volume effects in a good solvent. Expansion factors were considered to be equal in SLS and viscometry: $R_g/R_{g\theta} \approx ([\eta]/[\eta_\theta])^{1/3}$, where subscript θ denotes the θ-solvent. Then $\varepsilon = \frac{2a-1}{3}$, where a is the Mark-Kuhn exponent in $[\eta]=KM^a$. According to [25], in PMMA-acetone solutions a=0.72, A=1.5 nm, the Kuhn segment of PMMA consists of six monomer units.

Fig. 4a shows that experimental $R_g(M)$ of PMMAs and non-aggregated PMMA-Fs follow eq. (1) within a 10% accuracy. While comparing the results of calculation with the experimental R_g values, we must consider the PDIs of polymers, since R_g increases with PDI. From the Table 1 it follows that PDI≈1.65±0.15 for PMMA's, and for non-aggregated PMMA-Fs. Due to the independence of PDI on MW, a good correspondence of the experimental and calculated values of R_g was observed. In aggregated PMMA-Fs an interpretation of the scatter of R_{gs} is difficult due to the scatter of PDIs of individual macromolecules: according to Tab. 1, PDI =1.4 and 2.1 for PMMA-F_V and PMMA-F_{VI}, respectively. We have shown in Fig. 4a also the value of R_{gs}=63 nm determined for PMMA-F_{VII} in spite of the fact, that the fraction of small scatterers was too low in PMMA-F_{VII} to obtain their R_g.

Molar mass dependences of R_h and R_{hs} are also shown in Fig. 4b. (It should be noted, that in the dilute solutions of PMMA and of non-aggregated PMMA-Fs, R_h was found to be independent of q^2. Therefore, their PCS reflected the self-diffusion of macromolecules. In the PMMA-F_V and PMMA-F_{VI} solutions R_{hs} was also Independent of q^2. A slight q^2-dependence of R_{hs} in the PMMA-F_{VII} solution indicated the influence of internal motions within LA.)

The line in Fig. 4b presents the result of a linear fit $R_h \propto M^{0.36}$ for PMMA and non-aggregated PMMA-F. Fig. 4b shows that at equal MWs $R_{hs}<R_h$(PMMA). According to the theory [26, 27], this inequality could be due to the star-like structure of the multimers. If the multimers are star-like (Scheme 1), their aggregation number could be considered as the number of arms in the star. The ratio $h=f_{star}/f_{lin}$ of the friction coefficients of the star (f_{star}) and linear (f_{lin}) macromolecules of equal molecular masses is known [26] to decrease with the number of arms. For example, in three-functional stars h=0.947, in four-functional stars h=0.892 [26].

Since $R_h \propto f$ (see eq. (5), Section 4.2), $h=R_{hs}/R_h(PMMA)$. Therefore, from Fig. 4b we have got h=0.5, 0.9 and 0.8 for PMMA-Fs V-VII, respectively. The last two values are close to the predictions of h for four-armed stars. Unfortunately, the aggregation numbers k_s (Tab. 1) are too low to explain the observed lowering of h. On the other hand, in fluorinated polymers friction is reduced with respect to hydrocarbon polymers. Possibly, the fluorinated end-groups of the small scatterers can reduce f, since in the multimers they are located at the periphery of the coils.

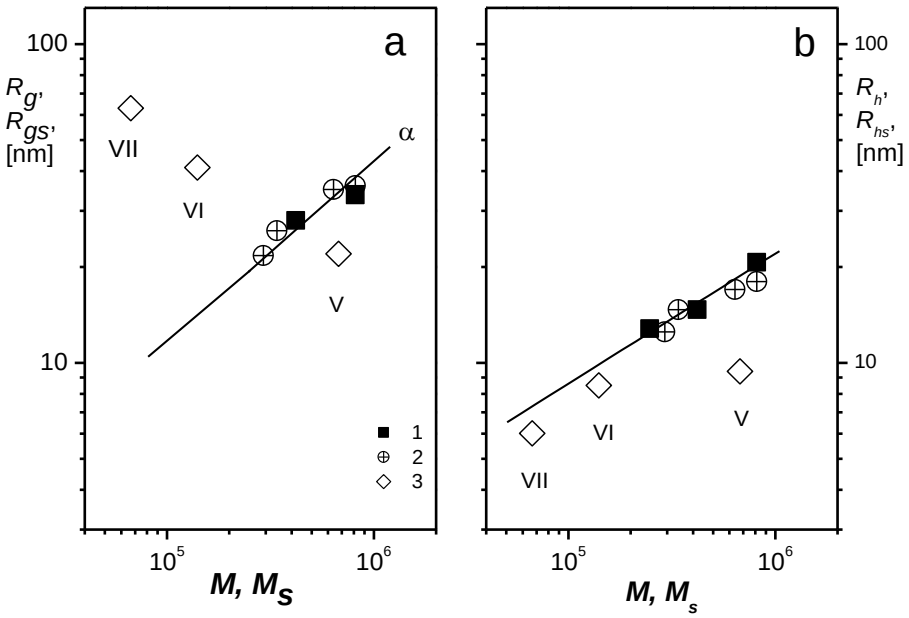

Fig. 4. Molecular-mass dependences of gyration and hydrodynamic radiuses of PMMA (1), of non-aggregated PMMA-F (2); and of the small scatterers of aggregated PMMA-Fs (3). Molecular masses were determined by SLS. In the last case the data was plotted vs. M_S. Line (a) is calculated according to eq. (1) for PMMA in acetone. Line is a linear fit of $R_h(M)$ for PMMAs and non-aggregated PMMA-Fs. Numbers V-VII indicate the numbers of PMMA-F samples (PMMA-F_V, PMMA-F_{VI}, and PMMA-F_{VII}, respectively).

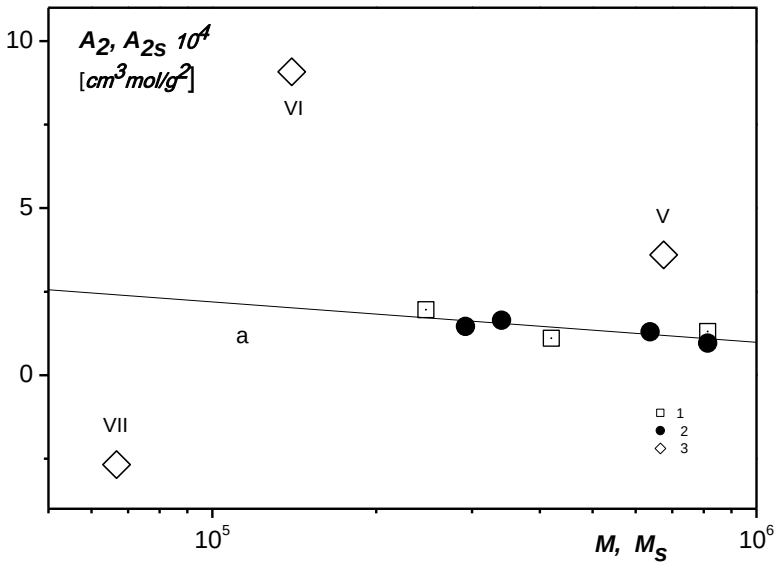

Fig. 5. Molar-mass dependences of second virial coefficients of acetone solutions of PMMA (1); non-aggregated PMMA-Fs (2); small scatterers of aggregated PMMA-Fs. Molar masses were obtained by SLS. Numbers V-VII indicate the number of PMMA-F sample as in Tab. 2).

Fig. 5 shows the molar mass dependences of A_2 of PMMA and non-aggregated PMMA-F in semi-lg coordinates. Line *a* presents the results of a linear fit in lg-lg coordinates: $A_2 \propto M^{-\gamma}$ (γ=0.37). This value of γ is at the upper end of the interval 0.14 < γ < 0.35 usual for flexible linear polymers [28].

Fig. 5 demonstrates A_{2s} plotted vs. M_s for aggregated PMMA-Fs. Fig. 5 shows that A_{2s} of PMMA-F_V and PMMA-F_{VI} are shifted up with respect to the line *a*. This indicates that the small scatterers are not individual PMMA-F macromolecules, but rather their low-order multimers: high A_{2s}-values of PMMA-F_V and PMMA-F_{VI} could manifest the repulsion between multimers. We see in Fig. 5 that A_{2s}(PMMA-F_{VI})>A_{2s}(PMMA-F_V). The same inequality was observed for the large scatterers of PMMA-F_{VI} and PMMA-F_V as described above. Thus the concentration dependence of the Zimm diagrams is influenced by the micelle repulsion in the whole range of scattering angles.

In PMMA-F_{VII} the negative virial term and/or the bridging between LAs are responsible for negative A_{2s}(PMMA-F_{VII}).

Summarizing the comparison of molar mass dependences of R_g, R_h and A_2 of PMMA and the small scatterers of aggregated PMMA-F, we see that the conformational, hydrodynamic, and thermodynamic parameters of the small scatterers are different from those of PMMA. Namely, R_{hs} was shown to be lower than R_h of the PMMA of the same MW. This can indicate the star-like nature of small scatterers (Scheme 1). A_{2s} of PMMA-F_V and PMMA-F_{VI} were shown to be larger than A_2 of corresponding PMMA, thus manifesting the repulsion between the low-order multimers. We have shown also that the end-groups of non-aggregated PMMA-Fs do not influence R_h, R_g, and A_2 of macromolecules.

Conclusions

A set of poly(methyl methacrylates) end-capped by [$Ge(C_6F_5)_3$] groups has been synthesized. Their self-assembly has been analyzed in acetone solutions at the room temperature by means of light scattering (SLS and PCS).

Upon decreasing MW, i.e. upon increasing the fraction of fluorinated component, aggregation of PMMA-F was shown to start. The first evidences of aggregation were observed already at M_{crit}=131000. In comparison, in the benzene solutions of polystyrenes end-capped with perfluoroalkyl groups $(CF_2)_{13}F$ M_{crit}=5000 [12]. Thus [$Ge(C_6F_5)_3$] groups are more effective in aggregation than perfluoroalkyl ones. One could suppose that π-π stacking interactions are responsible for the high aggregation ability of [$Ge(C_6F_5)_3$] groups.

Due to the high value of M_{crit}, the studied PMMA-Fs are the polymeric surfactants. This explains why their CACs were shown to be very low - lower than the concentration range of the light scattering study.

In aggregated PMMA-Fs the distributions of scatterers were found to be bimodal. The large aggregates, whose R_{hL} was much more than R_h of corresponding individual PMMA macromolecules, was observed. Existence of LA is inconsistent with the mean-filed theory, predicting only rather small spherical micelles at a low content of the aggregating component of a block-copolymer. Thus LAs indicate the super strong segregation limit proposed in [10].

We suppose that the distribution of scatterers in aggregated PMMA-Fs could be influenced by the fact, that PMMA-F is a mixture of polymers functionalized at one and two ends.

In aggregated PMMA-Fs the small scatterers were shown to have lower R_h and higher A_2 than corresponding individual PMMA of the same MW. Therefore, we believe that the small scatterers are not the individual macromolecules, but rather their low-order multimers.

At MW>M_{crit}, the molar mass dependences of R_h, A_2, R_g for non-aggregated PMMA-Fs have been shown to be the same as for PMMA. Hence, fluorinated end-groups do not influence the conformational and hydrodynamic behavior of non-aggregated PMMA-F.

Experimental

Synthesis

Poly(methyl methacrylates) were synthesized by radical polymerization in bulk, and in the chloroform and THF solutions at concentrations of methyl(methacrylate) 8.2, 3 and 2.6 mol/l, respectively. DAC (dinitrilazoisobutylic acid) was used as an initiator. In PMMA-Fs the chain transfer agent was $HGe(C_6F_5)_3$. PMMA-Fs of different MWs were obtained by changing the concentration of $HGe(C_6F_5)_3$ in the reaction media from 0.005 to 0.050 mol/l. The reaction was conducted at 60 °C up to a 10% conversion controlled by dilatometer. It is known that the polymerization kinetics permits the calculation of the content of polymers end-capped by one and by two ends [for example, 29]. According to [16], the relative constant of the chain transfer reaction is 0.3 for the radical polymerization MMA in the presence of $HGe(C_6F_5)_3$. Hence, the obtained PMMA-Fs contained 33 % of $(C_6F_5)_3Ge$-PMMA-$Ge(C_6F_5)_3$ and 67% of PMMA-$Ge(C_6F_5)_3$. Polymers were purified by triple precipitation from chloroform solutions into petroleum ether. After that the polymers were dried in vacuum at 40 °C.

Characterization

Mass-averaged molar mass (M_w) and polydispersity index PDI=M_w/M_n were determined by SEC. The Prominence LC-20VP device (Shimadzu) was used. It consisted of a water pump DGU-20A3, a hand injection system, a polystyrene-divinilbenzene columns (TSK-gel G600HXL and TSK-gel G5000 HXL of 10^5 -10^6 Å porosity), and a refractive index detector (RID-10A). The injector and column compartment were kept at 40 °C with the help of the thermostat CTO-20AC. THF was used as an eluent.

The flow rate was 5 ml/min. Molecular mass was determined using PMMA-standards (Fluka) of narrow polydispersity (PDI=1.02). Molar mass of PMMA-standards was varied from 5000 to 2000000. Each chromatogram of a PMMA-standard was carried out 4 times, and then an average chromatogram was obtained. The chromatograms were analyzed using a LC Solution-GPC software. The concentrations of injected polymer solutions were in the range 1÷5 g/L depending on the molar mass of polymer. The volume of injected solution was 20 mm^3. The presence of fluorinated groups in PMMA-F was checked by a spectrophotometric detector (SPD-20AV) at a wavelength λ=254 nm. At this λ the corresponding fluorinated homopolymer (PPG), had maximal adsorption [9].

In Tab. 2 the results of the SEC-characterization are presented for PMMA and PMMA-F. Molar fraction of fluorinated end groups was calculated as $m=1/N$, where $N=M_n(\text{SEC})/M_o$, where M_o is the MW of PMMA monomer unit.

Tab. 2. SEC characterization of the studied samples.

Sample	M_w [a]	PDI [b]	m [c] ,%
$PMMA_I$	830 000	1.8	0
$PMMA_{II}$	400 000	1.7	0
$PMMA_{III}$	200 000	1.7	0
$PMMA\text{-}F_I$	652 000	1.6	0.03
$PMMA\text{-}F_{II}$	521 000	1.7	0.03
$PMMA\text{-}F_{III}$	380 000	1.6	0.04
$PMMA\text{-}F_{IV}$	222 000	1.5	0.07
$PMMA\text{-}F_V$	131 000	1.4	0.10
$PMMA\text{-}F_{VI}$	51 000	2.1	0.41
$PMMA\text{-}F_{VII}$	43 000	1.8	0.43

[a] Weight-average molecular mass;
[b] $PDI=M_w/M_n$;
[c] Mole fraction of $[Ge(C_6F_5)_3]$ groups.

Light scattering was carried out at a wavelength λ=632.8 nm. A 20 mW Helium-neon laser was used as a source. The Photocor goniometer was used. The range of scattering angles was $30°<\theta<140°$. Second virial coefficients A_2, z-average gyration radiuses R_g, and M_w were determined by the double extrapolation procedure in Zimm coordinates:

$$Kc/\Delta R=P(q)^{-1}M^{-1}(1+2A_2c+\ldots) \quad (2)$$

Here $q=4\pi n_o \sin(\theta/2)/\lambda$ is the wave vector, n_o is the solvent refractive index;

$K=4(\pi n_s \nu)^2/N_A\lambda^4$ is the solution optical constant (N_A=Avogadro's number, ν=specific refractive index increment); ΔR is the excess Rayleigh ratio, $P(q)$ is the form-factor. At $qR_g<1$ $P(q)^{-1}= 1+q^2R_g^2/3$. While analyzing the aggregation, an apparent molar mass (M_{app}) is used: $1/M_{app}=Kc/\Delta R$.

The intensity scale was calibrated against toluene; ν was determined by an Abbe refractometer IRF-454B. PCS measurements were carried out simultaneously with the SLS ones. A 288-channel Photocor digital correlator with a logarithmic scale of sample times was used. Correlation functions of the scattered light intensity (I) were measured:

$$g^{(2)}_T(q,\tau)= \langle I(q,0)I(q,\tau)\rangle_T/\langle I(q)\rangle_T^2 \quad (3)$$

with τ being the delay time, T being the duration of measurements. Through the Ziegert relation, $g^{(2)}$ was converted into the first-order normalized electric field autocorrelation function

$$g^{(1)}(q,\Gamma)=\int G(\Gamma)e^{-\Gamma t}d\Gamma \quad (4)$$

where $G(\Gamma)$ is the distribution of decay rates. The translational diffusion coefficient D is expressed as

$$D(q)=<\Gamma>/q^2, \quad (5)$$

where $<\Gamma>=\int \Gamma G(\Gamma) d\Gamma$ is the mean decay rate. It is known that $D=kT/f$, where f is the friction coefficient, k is the Boltzmann constant, T is the temperature. According to the Stokes-Einstein relation, at infinite dilution

$$f=6\pi R_h \eta \quad (6)$$

where η is the solvent viscosity, R_h is the hydrodynamic radius of the equivalent hard sphere:

$$R_h=k_B T/6\pi D\eta \quad (7)$$

At $qR_h<1$ internal motions do not perturb the results. Hence, D (and R_h) are independent of q^2.

To obtain $G(\Gamma)$ from the correlation functions, in the DynaLS software the singular value decomposition procedure is combined with the non-negativity constraints on the solution. The problem of obtaining $G(\Gamma)$ is thus reduced to a least distance programming [30]. By variation of a regularization parameter the smoothness of distributions can be changed. Appropriate regularization parameter was chosen taking into consideration the randomness of residuals, and the reproducibility of results. In monomodal distributions the DynaLS analyses corresponds to the cumulant method. In bimodal distributions the comparison with a two-exponential fit has been done.

Prior to the experiments, scattering cells were washed with benzene, then they were vacuumized within 15 min, and after that they were filled with a dust-free air. The solutions were prepared at room temperature. Although the polymers dissolved within 10-15 minutes, all solutions were kept at least for 12 h before measurements, in order to ensure complete equilibration. Before the measurements, the solutions were clarified by filtering through Millipor-Millex PTFE filters of 0.45 μm porosity directly into dust-free cells. The solutions were kept at least 15 min in the PCS-device at 21 °C before the measurements. Temperature control was maintained within 0.1°. Equilibrium was ascertained by the constancy of the mean intensity of the scattered light during the measurements. Correlation functions were accumulated within 1÷5 min.

PCS was used as an express-method while choosing the selective solvent promoting the aggregation of [Ge(C_6F_5)] end groups. We compared the R_h-distributions of the model fluorinated polymer (PPG) in acetone, chloroform and THF solutions at room temperature. The R_h-distributions of PPG were shown to be bimodal. Fraction of LAs was dominating in acetone, whereas in THF it was almost absent. Chloroform solutions exhibited both fractions of comparable intensity. We shall report the details in the next article [17].

Acknowledgements

The financial support of RFBI grant 06-03-32872 is acknowledged.

References

[1] Pagliaro, M.; Ciriminna, R. *J Mater Chem* **2005**, *15*, 4981.
[2] Nostro, P.L. *Current Opinion in Colloid and Interface Science* **2003**, *8*, 223.
[3] Buhler, E.; Dobrynin, A.V.; DeSimone, J.M.; Rubinstein, M. *Macromolecules* **1998**, *31*, 7347.
[4] Hwang, H.S.; Heo, J.Y.; Jeong, Y.T.; Jin, S.-H.; Cho, D.; Chang, T.; Lim K.T. *Polymer* **2003**, *44*, 5153.
[5] Zhu, Sh.; Edmonds, W.F.; Hillmyer, M.A.; Lodge, T.P. *J Polym Sci Part B, Polym Phys* **2005**, *4*, 3685.
[6] Davidock, D.A.; Hillmyer, M.A.; Lodge, T.P. *Macromolecules* **2004**, *37*, 397.
[7] Lodge, T.P.; Hillmyer, M.A.; Zhou, Z. *Macromolecules* **2004**, *37*, 6680.
[8] Gasilova, E.R.; Koblyakova, M.A., Filippov, A.P.; Zakharova, O.G.; Zaitsev, S.D., Semchikov, Yu.D. *Polym Sci Ser A* **2006**, *48*, 989.
[9] Gasilova, E.R.; Zakharova, O.G.; Kozlov, A.V.; Filippov, A.P.; Semchikov, Yu.D. *Polym Sci Ser A,* in press.
[10] Semenov, A.N.; Nyrkova, I.A.; Khokhlov, A.R. *Macromolecules* **1995**, *28*, 7491.
[11] Lo Verso.; F, Likos, Ch.N. *Polymer* **2008**, *49*, 1425.
[12] Hems, W.P.; Yong, T.M.; van Nunen, J.L.M.; Cooper, A.I.; Holmes, A.B.; Griffin, D.A. *J Mater Chem* **1999**, *9*, 1403.
[13] Sawada, H.; Ikeno, K.; Kawase, T. *Macromolecules* **2002**, *35*, 4306.
[14] Yusa, Sh.; Yamamoto, T.; Hashidzume, A. *Polym Journal* **2002**, *34*, 117.
[15] Zaitsev, S.D.; Turshatov, A.A.; Pavlov, G.M.; Semchikov, Yu.D.; Bochkarev, M.N. *Polym Sci Ser B* **2004**, *42*, 241.
[16] Zakharova, O.G.; Zaitsev, S.D.; Semchikov, Yu.D.; Smirnova, N.N.; Markin, A.V.; Bochkarev, M.N. *Polym Sci Ser A* **2005**, *47*, 901.
[17] Gasilova, E.R. *unpublished results*.
[18] Zakharova, O.G.; Zaitsev, S.D., Gushchina Y.Y.; Semchikov Y.D.; Gusev S.I. *Polym Sci Ser B* **2005**, 47, 146.
[19] Eskin, V.E. *Light Scattering from Polymer Solutions and Properties of Macromolecules*, Leningrad, Science, **1986**.
[20] Huglin, M.B. *Light Scattering from Polymer Solutions*, Academic Press, London NJ, **1972**.
[21] Kostacis, K.; Mourmouris, S.; Charalabidis, D.; Pitsikalis, M. *Eur Phys J E* **2003**, 10, 55.
[22] Liu, F., Frer, Y.; Francois, J. *Polymer* **2001**, *42*, 2969.
[23] Kelarkis, A.; Havredaki, V.; Yuan, X.F.; Yang, Y.W.; Booth, C. *J Mater Chem* **2003**, *13*, 2779.
[24] Benahmed**,** A.; Ranger, M.; Leroux, BJ-Ch. *Pharmaceutical Research* **2001,** *18*, 323.
[25] Tsvetkov, V.N.; Eskin V.E.; Frenkel S.Y. *Structure of Macromolecules in Solutions,* Moscow, Science, **1964**.
[26] Yamakwa, H. *Modern Theory of Polymer Solutions*. New York, Harper & Row, **1971**.
[27] Burchard, W. *Adv Polym Sci* **1999,** *143*, 112.
[28] Isihara, A.; Koyama, R.J. *J Chem Phys* **1956**, 25, 712.
[29] Gatalgil-Giz, A.; Giz, A.; Oncul-Koc, A. *Polym Bull* **1999,** *43*, 215.
[30] Lowson, C.L.; Hanson R.J., *Solving Least Squares Problems*, Englewood Cliffs, NJ: Prentice Hall, **1974**.